REPORT
doi:10.26443/seismica.v4i2.1771

Supershear source model of the 2025 M7.8 Myanmar earthquake and paleoseismology of the Sagaing Fault: regions of significant overlap with past earthquakes

D. Melgar *[1], **R. Weldon**[1], **Wang Y.**[2], **M.G. Bato**[3], **L.T. Aung**[4], **Shi X.**[5], **W. Wiwegwin**[6], **S.N. Khaing**[7], **S. Min**[8], **M. Thant**[9], **C.M. Speed**[3], **R. Zinke**[3], **E.J. Fielding**[3], **A.J. Meltzner**[4,10], **T. Dawson**[11]

[1]Department of Earth Sciences, University of Oregon, Eugene, OR, USA, [2]Department of Geosciences, National Taiwan University, Taipei, Taiwan, [3]Jet Propulsion Laboratory, California Institute of Technology, Pasadena, CA, USA, [4]Earth Observatory of Singapore, Nanyang Technological University, Singapore, [5]Zhejiang University, Hangzhou, China, [6]Department of Mineral Resources, Bangkok, Thailand, [7]Department of Geology, Hinthada University, Myanmar, [8]Department of Geology, Banmaw University, Myanmar, [9]Myanmar Institute of Earth and Planetary Sciences, and University of Yangon, Myanmar, [10]Asian School of the Environment, Nanyang Technological University, Singapore, [11]California Geological Survey, San Mateo, CA, USA

Author contributions: *Conceptualization*: D.M., R.W.,Y.W., M.G.B., L.T.A.,X.S.,W.W. *Formal analysis*: All authors. *Software*: D.M., M.G.B., C.M.S., R.Z., E.J.F. *Visualization*: D.M., R.W., W.Y., L.T. *Funding Acquisition*: D.M., R.W., M.G.B., Y.W.,X.S. *Writing – original draft*: D.M., R.W. *Writing – review & editing*: All authors.

Abstract The 2025 Mw 7.8 earthquake on the central Sagaing Fault is one of the most destructive seismic events in Myanmar's recorded history, producing near-fault shaking exceeding Modified Mercalli Intensity X and impacting tens of millions of people across Southeast Asia. We present a detailed kinematic rupture model of the event based on joint inversion of regional strong motion waveforms and Sentinel-1 SAR pixel offsets. The rupture extended over ~450 km with an average slip of 3–5 m, predominantly within the upper 10 km of the crust. Inversions favor a maximum rupture speed of ~4.8 km/s, consistent with supershear propagation inferred from near-field waveform observations. We also report on paleoseismic evidence from a key site at the epicenter of the 2025 earthquake near Mandalay, which reveals five surface-rupturing earthquakes over the past millennium, with similar average displacement. Our results indicate a pattern of overlapping large ruptures along the central fault, with implications for rupture segmentation, recurrence, and seismic hazard. Given the exceptional exposure to earthquakes and high strain rates, our findings underscore the need for urgent attention to earthquake preparedness and infrastructure resilience in central Myanmar.

Burmese စစ်ကိုင်းပြတ်ရွှေ့အလယ်ပိုင်းတွင် ဗဟိုပြုလျှပ်ခတ်ခဲ့သော ပင်းအား ၇.၈ အဆင့်ရှိ ၂၀၂၅ လျှင်သည် မြန်မာ့လျှင်သမိုင်းမှတ်တမ်းတွင် အပျက်အစီးအကြီးများဆုံးလျှင်များထဲမှ တစ်ခုဖြစ်ပြီး ပြတ်ရွှေ့အနီးတလျှောက်တွင် လျှင်ဒါဏ်ခံစားရမှု မာကယ်လီ စကေး ၁၀ အထက်ရှိကာ၊ အရှေ့တောင်အာရှတစ်လွှားရှိ လူဦးရသေန်းပေါင်းများစွာ အပေါ်ကို သက်ရောက်မှုရှိခဲ့သည်။ ဆန်တီနယ်-၁ ဂြိုလ်တုပုံရိပ်များ၏ (Sentinel-1 SAR pixel offsets) ပုံရိပ်အစက်အပြောက်အရွှေ့များနှင့် ဒေသတွင်းလျှင်လှိုင်းမှတ်တမ်းများကို အခြေခံပေါင်းစပ်အသုံးပြု၍ ယခုလျှင်၏ မြေပြင်ရွှေ့ပြတ်မှုအသေးစိတ်ပုံစံကို သုံးသပ်တင်ပြထားပါသည်။ မြေပြင်ရွှေ့ပြတ်မှုသည် ကမ္ဘာ့အပေါ်ယံလွှာ၏ ၁၀ ကီလိုမီတာအတွင်းတွင် ပျမ်းမျှအရွှေ့ ၃ - ၅ မီတာခန့်ရှိပြီး အရှည်အားဖြင့် ၄၅၀ ကီလိုမီတာဝန်းကျင်ခန့်အထိ ရွှေ့ပြတ်မှု ဖြစ်ခဲ့သည်။ လျှင်လှုပ်ခတ်သော ပြတ်ရွှေ့အနီး တိုင်းတာမှတ်တမ်းတင်ထားသော လျှင်လှိုင်းများကို လေ့လာဆန်းစစ်မှုများအရ အမြင့်ဆုံးရွှေ့ပြတ်နှုန်းသည် ၁ စက္ကန့်တွင် ၄.၈ ကီလိုမီတာ နှုန်းဖြင့် ရွှေ့ပြတ်ခဲ့သကောင့်၊ မြန်နှုန်းမြင့်သော ဖျက်အားပြင်းလျှင် အမျိုးအစားဖြစ်ကောင်း ကောက်ချက်ချနိုင်သည်။ မနှစ်တလေးမြို့အနီး ၂၀၂၅ ခုနှစ်လျှင်ဗဟိုချက်ဝန်းကျင်ရှိ အဓိကနရောမှ အတိတ်လျှင်ဆိုင်ရာ အထောက်အထား မှတ်တမ်းများအရ လွန်ခဲ့သော ထောင်စုနှစ်အတွင်း မျက်နှာပြင်ရွှေ့ပြတ်မှုရှိခဲ့သော လျှင်များ အနည်းဆုံး ငါးကြိမ်ခန့် လှုပ်ခတ်ခဲ့ပြီး တူညီသော ပျမ်းမျှရွှေ့ပြတ်မှုပမာဏရှိခဲ့သည်ကိုလည်း တွေ့ရသည်။ ကျွန်ုပ်တို့၏လေ့လာတွေ့ရှိချက် ရလဒ်များသည် ပြတ်ရွှေ့အေဆစ်အပိုင်းများ ပိုင်းခြားသတ်မှတ်ခြင်း၊ လျှင်များ ပန်းလည်လှုပ်ခတ်မှုအချိန်ကာလ နှင့် ပင်းအားပမာဏ၊ လျှင်အနှုတရာယ် စသည့်အကျိုးသက်ရောက်မှုများနှင့်အတူ စစ်ကိုင်းပြတ်ရွှေ့၏ အလယ်ပိုင်းတလျှောက်တွင် ပမာဏကြီးများရှည်လျားသော လျှင်ရွှေ့ပြတ်မှု၊ ပြတ်ရွှေ့အေဆစ်အပိုင်းများ တစ်ခုနှင့်တစ်ခုထပ်နသေသော ပုံစံကို လေ့လာတွေ့ရှိရသည်။ လူဦးရ၊ အဆောက်အဦ၊ အခြေခံအဆောက်အအုံများ အလွန်မြင့်မားမှု၊ စစ်ကိုင်းပြတ်ရွှေ့ တစ်လျှောက် ပုံပျက်ယွင်းမှုနှုန်း မြင့်မားခြင်းတို့ကြောင့် မန္တလေးနိုင်ငံတွင် လျှင်ဘေးအန္တရာယ် လျှော့ကျရေးဆိုင်ရာ ကြိုတင်လေ့ကျင့် ပြင်ဆင်မှုနှင့် အခြေခံအဆောက်အအုံများ၏ ခံနိုင်ရည်ရှိရေးတို့အား အရေးပေါ်အဆင့် အာရုံစိုက်ဆောင်ရွက်ရန် လိုအပ်ကြောင်း ကျွန်ုပ်တို့၏ လေ့လာတွေ့ရှိချက်များက ညွှန်းဆိုနသေည်။

Production Editor:
Tiegan Hobbs
Handling Editor:
Kiran Kumar Thingbaijam
Copy & Layout Editor:
Hannah F. Mark

Signed reviewer(s):
Kiran Kumar Thingbaijam

Received:
June 4, 2025
Accepted:
July 18, 2025
Published:
July 31, 2025

*Corresponding author: dmelgarm@uoregon.edu

Thai เมื่อวันที่ 28 มีนาคม 2568 เกิดแผ่นดินไหวขนาด 7.8 ตามมาตราโมเมนต์ (Mw) มีสาเหตุเกิดจากการเลื่อนตัวของรอยเลื่อนสะกาย ถือเป็นหนึ่งในเหตุการณ์แผ่นดินไหวที่สร้างความเสียหายมากที่สุดในประวัติศาสตร์ของประเทศเมียนมา โดยมีระดับความรุนแรงของแผ่นดินไหวมากกว่าระดับ X ตามมาตราเมอร์คัลลี่ดัดแปลง (Modified Mercalli Intensity) ในบริเวณใกล้กับตำแหน่งของรอยเลื่อนสะกาย แรงสั่นสะเทือนของแผ่นดินไหวสามารถรับรู้ได้ในหลายประเทศและส่งผลกระทบต่อประชากรนับสิบล้านคนในภูมิภาคเอเชียตะวันออกเฉียงใต้ ผลการศึกษานี้ได้เสนอแบบจำลองการเกิดแนวรอยแตกของพื้นผิวดินด้วยการวิเคราะห์จลนศาสตร์แบบผกผัน (kinematic rupture model) โดยอาศัยข้อมูลคลื่นสั่นสะเทือนของพื้นดินที่ถูกบันทึกจากสถานีตรวจวัดแผ่นดินไหวในภูมิภาค และข้อมูลการเปลี่ยนรูปของพื้นผิวดินจากดาวเทียม Sentinel-1 ผลการวิเคราะห์พบว่าแนวรอยแตกของพื้นผิวดินจากเหตุการณ์แผ่นดินไหวมีระยะทางประมาณ 450 กิโลเมตร มีระยะการเลื่อนตัวเฉลี่ยอยู่ที่ 3–5 เมตร และส่วนใหญ่จะเกิดขึ้นในชั้นเปลือกโลกส่วนบนที่ความลึกไม่เกิน 10 กิโลเมตร การเลื่อนตัวของแนวรอยแตกมีความเร็วสูงสุดประมาณ 4.8 กิโลเมตรต่อวินาที ซึ่งสอดคล้องกับรูปแบบการเกิดแผ่นดินไหวที่มีความเร็วของแนวรอยแตกเหนือความเร็วเฉือน (supershear) คณะผู้ศึกษายังพบหลักฐานการเกิดแผ่นดินไหวโบราณอย่างน้อย 5 เหตุการณ์ ในช่วง 1,000 ปีที่ผ่านมา ในร่องสำรวจใกล้เมืองมัณฑะเลย์ซึ่งเป็นตำแหน่งของศูนย์กลางของแผ่นดินไหวครั้งนี้ โดยเหตุการณ์แผ่นดินไหวโบราณดังกล่าวทำให้เกิดระยะการเลื่อนตัวของรอยเลื่อนในแต่ละครั้งมีระยะทางที่ใกล้เคียงกัน ผลการศึกษาในครั้งนี้ยังบ่งชี้ให้เห็นถึงรูปแบบของการเกิดแผ่นดินไหวขนาดใหญ่ในพื้นตอนกลางของแนวรอยเลื่อนสะกาย และสามารถนำไปใช้ประโยชน์ในการกำหนดตำแหน่งของรอยเลื่อนย่อย การเกิดแผ่นดินไหวซ้ำ และการประเมินภัยพิบัติแผ่นดินไหว บริเวนตอนกลางของประเทศเมียนมา เป็นพื้นที่เสี่ยงภัยจากแผ่นดินไหวสูง เนื่องจากมีสิ่งก่อสร้าง อาคาร และผู้คนอาศัยอยู่เป็นจำนวนมาก และมีอัตราการการเปลี่ยนรูปของหินหรือชั้นเปลือกโลกที่สูง ดังนั้น จึงมีความจำเป็นเร่งด่วนที่จะต้องให้ความสำคัญต่อการเตรียมความพร้อมรับมือแผ่นดินไหว และการเสริมสร้างความมั่นคงแข็งแรงของโครงสร้างพื้นฐานในบริเวณดังกล่าว

Simplified Chinese 2025 年发生于实皆断层中段的曼德勒地震 (Mw 7.8) 是缅甸历史上最严重的灾害性地震之一。该地震造成断层周边地区的强烈地动——修订麦卡利震度分级 (MMI) 达 10 级以上，并对东南亚地区上千万人产生重要影响。本研究透过强震地震波形与哨兵一号卫星合成孔径雷达像素偏移资料进行联合反演，建立本次地震的断层破裂运动模型。研究成果表明，本次地震的同震位移达 3-5 米，破裂长度超过 450 公里，主要破裂集中在地壳浅部 10 公里内的断层面上。模型中最大地震破裂传播速度可达~4.8 公里/秒，与近断层的地震波观测资料所指出的超剪切地震传播型态相符。而位于 2025 年地震震中附近的古地震探槽也发现：该段断层在过去约 1000 年期间中发生了至少 5 次的地表破裂事件，且每次事件均具有相似的同震位错量。我们的古地震研究成果揭示，实皆断层中段具有大型的重叠破裂特性，对该断层的孕震区段、破裂周期和地震灾害分析都有一定程度的影响。鉴于缅甸中部的高地震风险程度与高应变率，本研究认为该地区的基础建设韧性与地震灾害防备亟需特别关注。

Non-technical summary On March 28, 2025, a powerful magnitude 7.8 earthquake struck central Myanmar along the Sagaing Fault, causing severe shaking near the fault and damage as far away as Bangkok, Thailand. Nearly 18 million people experienced strong shaking, and while the official death toll is around 4,000, the true number is much higher due to limited access and reporting in conflict zones. Using ground sensors and satellite data, scientists found the rupture extended about 450 kilometers with 3-5 meters of movement along the fault. The fault broke at unusually high speed—a phenomenon called "supershear"—which can generate especially strong shaking. Trenches dug across the fault in 2016 & 2018 revealed that this same section has broken in multiple past earthquakes, including in 1839, and the 1946/1956 sequence. These findings show that large earthquakes repeatedly strike this part of the fault. Because the region is heavily populated and rapidly developing, the Sagaing Fault remains a major hazard. Improving construction standards, emergency preparedness, and continued research are essential to reduce future risk.

1 Overview of the event and the Sagaing fault

The 2025 Mw 7.8 Myanmar earthquake (Inoue et al., 2025; Kearse and Kaneko, 2025; Ye et al., 2025) represents a landmark event in the seismic history of the country and the broader Southeast Asian region (Wang et al., 2014; Thein et al., 2009; Hurukawa and Maung, 2011). The U.S. Geological Survey's ShakeMap (U.S. Geological Survey Hazards Program, 2017, Figure 1A) shows that near-fault areas experienced extreme shaking, with Modified Mercalli Intensity (MMI) levels exceeding MMI X, causing widespread destruction. The event's regional importance is underscored as well by the high population densities surrounding the fault; according to the PAGER system (Prompt Assessment of Global Earthquakes for Response; Earle et al., 2009; Wald et al., 2010), and also from the USGS which estimates human and economic impacts, approximately 17.8 million people were exposed to shaking of MMI VII or greater, and 6.2 million people to MMI IX or greater (U.S. Geological Survey, 2025). The shaking was so intense that damage and strong ground motions were reported as far away as Bangkok, Thailand. At the time of this writing, official fatality counts are approximately 4,000. However, given the extraordinary exposure to severe shaking, and known structural vulnerabilities in Myanmar and neighboring regions, it is likely that the true number of fatalities is significantly larger. This is especially true because of the complicating factor of ongoing issues in the area that impair accurate reporting and emergency response—it is well-established that impacts from natural disasters in areas experiencing instability are systematically under-reported (e.g. National Research Council, 2007).

Myanmar occupies a geologically complex and tec-

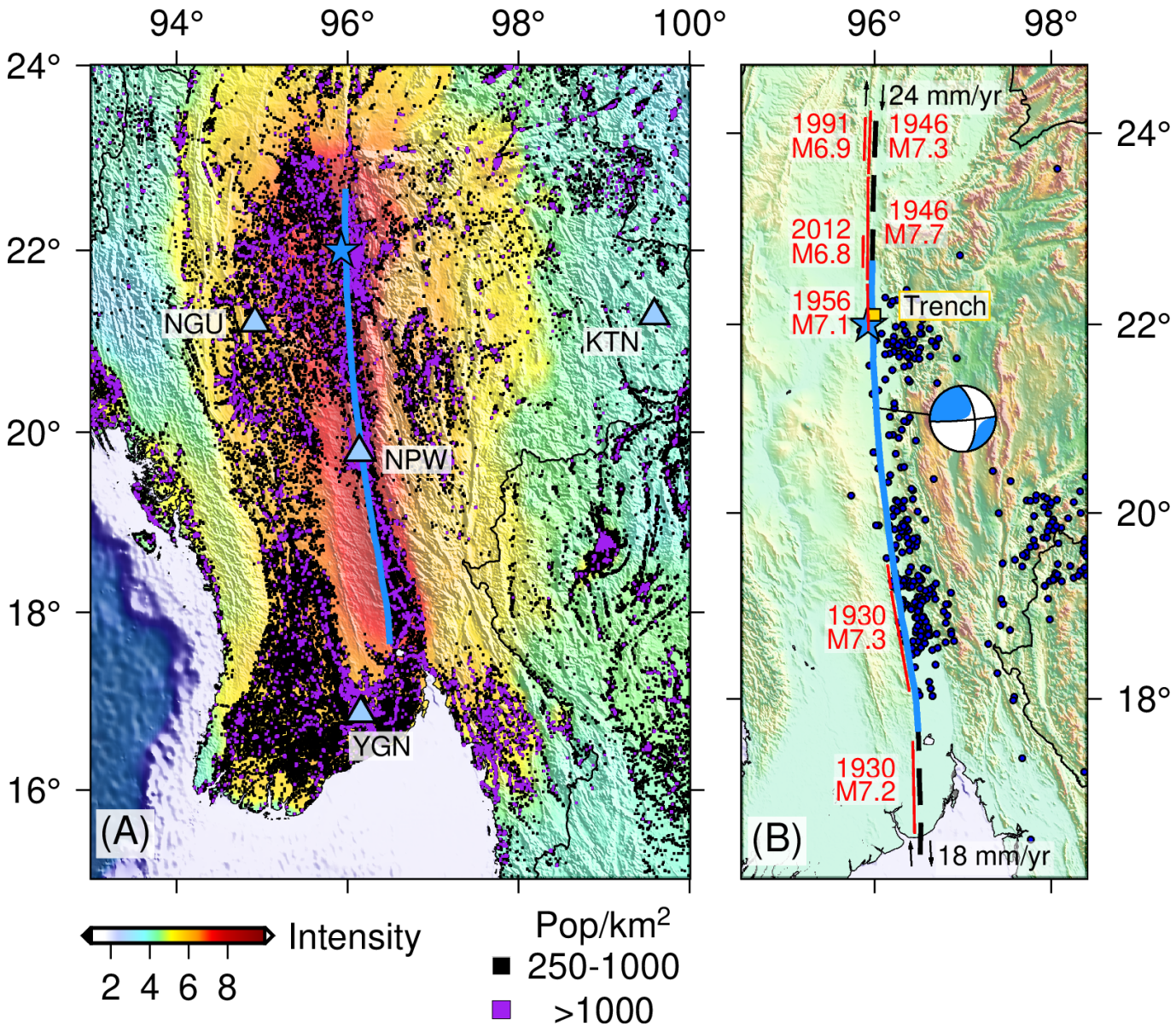

Figure 1 (A) Overview of shaking intensity from USGS ShakeMap (U.S. Geological Survey Hazards Program, 2017) and impacts to population from the M7.8 earthquake. The triangles are the stations used for inversion, the star is the event hypocenter, and the blue line the assumed surface trace of the rupture. Population density data is from LandScan (Lebakula et al., 2024). (B) Tectonic overview of the Sagaing Fault: past ruptures estimated lengths are from Wang et al. (2014), blue star is the event hypocenter, moment tensor for the mainshock is from the global CMT project (Ekström et al., 2012), and 2 weeks of aftershocks are from the Thailand National Seismic Network (Pornsopin et al., 2023). Shown as well are the slip-rate estimate for the Sagaing Fault from Tin et al. (2022) and the location of our trench site (yellow square) used to establish the paleoseismic history of the fault in this work.

tonically active region (Figure 1B) at the intersection of the Indian, Sunda, and Eurasian plates (e.g., Socquet et al., 2006; Gahalaut and Gahalaut, 2007). The oblique convergence between the Indian and Sunda plates is accommodated by a combination of subduction, strike-slip faulting, and block extrusion processes (Wang et al., 2014; Shi et al., 2018; Mallick et al., 2019). To the west, the Rakhine-Bangladesh megathrust marks the zone of north-eastward subduction of the Indian plate beneath the Burma plate, forming the Indo-Burman ranges. To the east, the prominent right-lateral Sagaing Fault (on which the 2025 event occurred) serves as the principal tectonic boundary (Socquet et al., 2006; Wang et al., 2014; Mallick et al., 2019; Tin et al., 2022; Lindsey et al., 2023). Between these two major structures lies the Central Myanmar Belt (CMB), an elongate lowland region bounded by active deformation on both sides. Geodetic measurements show that the Indian Plate is moving northeastward relative to the Sunda plate at a rate of approximately 35 mm/yr near 10°N, with the Sagaing Fault accommodating 18–24 mm/yr of right-lateral strike-slip motion (Steckler et al., 2016; Tin et al., 2022; Lindsey et al., 2023). The remaining convergence is partitioned across the Rakhine-Bangledsh megathurst, the Indo-Burman fold and thrust belt, and the Central Myanmar Belt west of the Sagaing Fault. Historical and instrumental records indicate that the region can produce large and damaging earthquakes, posing signifi-

cant seismic hazards, especially for rapidly growing urban centers like Yangon, Nay Pyi Taw, and Mandalay (e.g. Le Dain et al., 1984; Xiong et al., 2017; Hurukawa and Maung, 2011).

The Sagaing Fault is a major north-south striking right-lateral strike-slip fault extending over 1,200 km from the Andaman Sea in the south to the eastern Himalayan syntaxis in the north (e.g., Maung, 1987; Curray, 2005). It accommodates the primary component of dextral shear between the Burma and Sunda plates. Formed most likely in the late Oligocene (Morley and Arboit, 2019), the fault has recorded a cumulative displacement of 330–450 km (e.g., Maung, 1987; Wang et al., 2011; Xiong et al., 2017; Tun and Watkinson, 2017). Modern GNSS observations reveal that the fault's slip rate varies along strike, with 23–24 mm/yr measured along central segments and somewhat slower rates (~16 mm/yr) inferred for southern segments with workers suggesting potentially variable dips from subvertical to vertical along-strike (Mon et al., 2020; Tin et al., 2022; Yang et al., 2024). The fault is segmented into several distinct sections, including the Sagaing, Meiktila, and Bago segments in the south (e.g. Wang et al., 2014; Panda et al., 2018; Tin et al., 2022; Tun and Watkinson, 2017). Each segment exhibits varying degrees of locking and strain accumulation at depths of 10–16 km (Socquet et al., 2006; Maurin et al., 2010; Tin et al., 2022; Vigny et al., 2003). Stress transfer modeling over the past century, and the instrumental seismic catalog, have identified seismic gaps along the central and southern Sagaing Fault. Models of the interseismic velocity field from space geodesy show these gaps are most likely coupled and not creeping (Tin et al., 2022): these are regions of heightened seismic hazard. Notable historical earthquakes, such as the 1930 Bago, 1946 Sagaing, and 2012 Thabeikkyin earthquakes, underscore the fault's potential to produce large-magnitude events (Wang et al., 2014; Hurukawa and Maung, 2011).

In this fast report we highlight how the 2025 rupture fits within this broader tectonic history for the region by producing a detailed kinematic slip model based on joint inversion of regional strong motion data and remote sensing observations. We will discuss findings from trenches near the epicenter of the 2025 rupture which have evidence of the 1839 M7.7 and the 1946/56 M7.7/7.1 sequence and re-ruptured again during the 2025 event.

2 Available Data and Methods

2.1 Regional Seismic Data

Three-component strong motion recordings from four regional stations (Figure 1A), were processed to obtain ground displacement time series (see Data Availability). Raw acceleration data were first corrected for instrument gain using known calibration factors. Each component was then baseline-corrected and de-trended to remove any DC offset. To reduce long-period drift and high-frequency noise, we applied a zero-phase, 4-pole Butterworth bandpass filter with corner frequencies at 0.05 Hz and 0.4 Hz. The filtered acceleration time series were then numerically integrated twice—first to determine velocity, then to displacement—using trapezoidal integration. This process yielded waveforms which were then decimated from their native sample rates of 100 and 200 Hz down to 5 Hz, suitable for kinematic slip inversion. The farthest station, KTN, is ~370 km from the surface trace of the Sagaing Fault while the closest site, NPW, in the capital city of Nay Pyi Taw, is only 2.5 km from the surface trace (Figure 1A).

NPW is particularly important because of its proximity to the fault (Figure 1A, 2); however, the network operator reported that approximately 3 days before the mainshock the station's GNSS antenna stopped working and the station lost absolute time (Lai et al., 2025). This means that without some form of calibration the data cannot be used for slip inversion. To correct for this, we use eight Mw>4.5 events that occurred in the vicinity of the mainshock hypocenter (Figure 1B) in the 5 years prior and for which absolute timing at the site is available. We picked the P-wave arrivals at NPW for each of these eight events and estimated the theoretical P-wave arrival times by ray tracing from the catalog hypocenter to the location of NPW through a layered Earth model. We then obtain a "station delay" by taking the difference between the observed P-wave arrival time, t_{obs}, and the expected or modeled P-wave arrival time, t_{mod}. We noted that the delays are correlated to the station-event distance, so we also regressed for the best fit straight line of the station delays as a function of hypocentral distance. This linear model then allowed us to solve for the estimated theoretical arrival of the P-wave from the 2025 mainshock (red triangle in Figure S1) given its known hypocentral distance of 240 km. We compared this expected arrival to the observed arrival (yellow square in Figure S1). In this analysis we used three different velocity models: two global ones, PREM and IASP91 (Dziewonski and Anderson, 1981; Kennett and Engdahl, 1991); and a regional lithospheric model (Pasyanos et al., 2014). We found that, while there are slight variations between velocity models, for all three the difference between the observed and expected P-wave arrival time for the 2025 mainshock is <1 s. From this we concluded that station NPW can be reliably used for slip inversion without further correction. This finding is consistent with Lai et al. (2025) who performed a similar analysis on other regional events and correlation of seismic noise and concluded likewise, that the station's clock had drifted no more than 1s from the time the GNSS clock malfunctioned to the time of the mainshock.

2.2 Space geodetic data

We employed two sources of space geodetic data to estimate the coseismic displacements. First, we used near-infrared (band 8) optical imagery from the European Space Agency (ESA) Copernicus Sentinel–2 Level 1C satellite imagery products (Drusch et al., 2012). We obtained north-south and east-west displacements by pixel offset tracking using two or more ortho-rectified and co-registered images acquired at different times (e.g., between 28 February and 6 April, 2025). To iden-

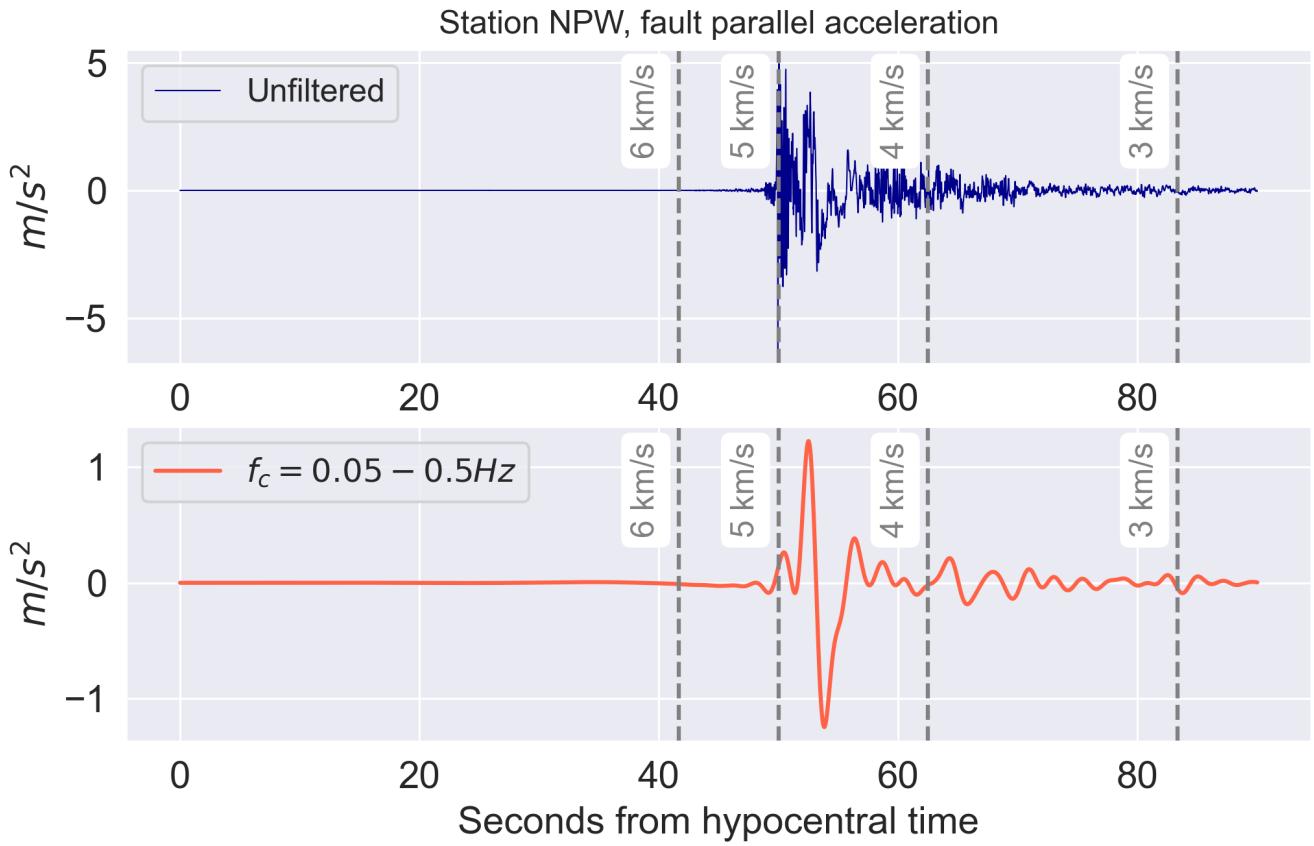

Figure 2 Strong motion data from station NPW (location in Figure 1A). Plotted is the fault-parallel acceleration, assuming a strike angle of 355°, without filtering and with a band pass filter applied. The main acceleration pulse is interpreted as the rupture transiting along the Sagaing Fault on the segment closest to NPW. Dashed lines represent rupture velocities needed for the rupture pulse to reach NPW at specific times.

tify the shift in surface features between the images, we used the autonomous Repeat Image Feature Tracking (autoRIFT) software (Gardner et al., 2018; Lei et al., 2021) that measures offsets in the image row (north-south) and column (east-west) directions. These offsets, initially in pixel units, are then converted to ground displacements by multiplying them by the known pixel size (i.e., 10 meters for Sentinel-2 band 8). The result is a two-dimensional horizontal displacement field representing surface motion in the east-west and north-south directions. This technique is especially useful for mapping large, coherent motions such as glacier flow, landslides, or volcanic deformation. Though it is less precise than radar-based displacement-retrieval methods like radar interferometry (e.g. Strozzi et al., 2002; Casu et al., 2011), pixel tracking is more sensitive to north-south displacement and does not decorrelate in high-strain regions near the fault rupture (e.g., Avouac and Leprince, 2015). While we did not use these displacement data in the inversion, they were used early on to determine the surface trace of the rupture and build the inversion geometry shown in Figure 1A,B.

Next, we utilized two pairs (Figure 3) of synthetic aperture radar (SAR) images from the European Space Agency's (ESA) Copernicus Sentinel-1A/B satellites—one pair for each track (ascending Track 143 and descending Track 106)—that captured the earthquake event. We measured the pixel offsets in both the range (across-track) and azimuth (along-track) directions using the Ampcor module within the ISCE2 software package (Rosen et al., 2012). The pre- and post-earthquake Sentinel-1 Level-1 Single Look Complex (SLC) images were first co-registered using available restituted orbit files. We performed cross-correlation between image patches in the reference and secondary scenes to determine sub-pixel shifts in both the range and azimuth directions. The measured offsets, initially in image coordinates, were converted to ground displacements using the sensor's known viewing geometry and pixel spacing. Range offsets correspond to displacements in the radar line-of-sight (LOS) direction, which has a strong east-west component for Sentinel-1's near-polar orbits and can include contributions from vertical land motion, while azimuth offsets capture motion along the satellite's trajectory and are primarily dominated by north-south deformation. Given the dextral north-south style of faulting, we prioritized the azimuth offsets. The resulting horizontal displacement fields are particularly robust for measuring large, decorrelating motions—such as coseismic rupture, glacier flow, volcanic deformation, and landslides—that may not be reliably captured with conventional interferometric phase techniques (e.g., Pathier et al., 2006; Casu et al., 2011; Lei et al., 2021; Bato et al., 2021).

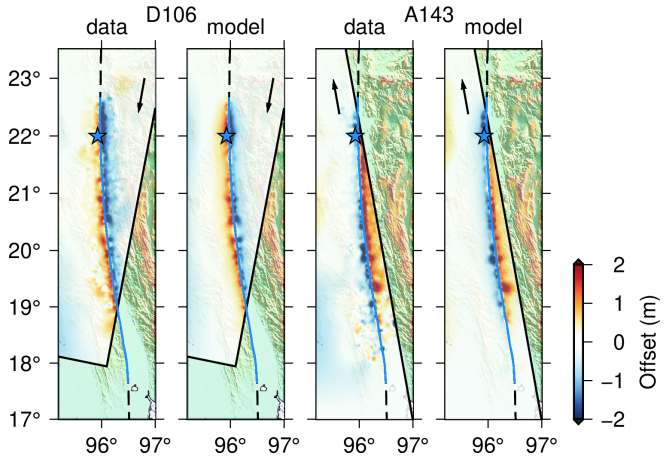

Figure 3 Azimuth pixel offsets from SAR ascending track 143 and descending track 106. The blue line is the assumed fault trace and the star is the event hypocenter. The arrow in each scene indicates the satellite flight path, and the offset displacement is thus the dot product of the horizontal coseismic deformation with this unit vector.

2.3 Kinematic Inversion

The first step in the kinematic inversion is defining the fault geometry. We used the Sentinel 2 optical imagery pixel offsets, as noted in Section 2.2, to define the surface expression of the fault (blue line in Figure 1A, B) and the first 2 weeks of aftershocks from the Thai regional network (Pornsopin et al., 2023, Figure 1B) to define the approximate extent of faulting. We note that the aftershock locations are biased east of the surface trace, which is most likely an artifact because one-sided networks with large azimuthal gaps can have systematic biases like these (e.g. Bondár et al., 2004). We assumed a seismogenic depth (the maximum extent of slip) of 20 km in line with other reports (e.g. Tun and Watkinson, 2017; Tin et al., 2022) that determined locking depths from seismicity and inversions of regional GNSS measurements of the interseismic velocity field. Finally, we discretized the fault into triangular subfaults using a 3D finite element meshing software. To account for the depth dependent resolution of slip inversions (e.g. Xu et al., 2016) we used progressively coarsening subfaults with depth. From 0 to 2.5 km subfaults have ~4 km vertices, from 2.5 to 10 they have ~7 km vertices, and from 10 to 20 km they have ~10 km vertices. For simplicity, we first assumed a vertical dip; this geometry can be seen in Figure 4A. Additionally, we built a second "variable dip" geometry based on the geodetic inversion results of Tin et al. (2022), which concluded that the interseismic velocity field was best explained by a fault that had vertical dip south of ~20°N, a 78° westward dip between ~20°N and ~21.5°N and then a 71° eastward dip nort of 21.5°N. We produced kinematic models on this "corkscrew" geometry to test whether the data preferred one or the other. This geometry can be seen in Figure 4B, and each model has ~850 subfaults. For each geometry elastostatic and elastodynamic Green's functions are generated using the frequency-wavenumber approach of Zhu and Rivera (2002) and the regional LITHO1.0 model discussed in Section 2.1.

We carry out kinematic slip inversion using the multi-time-window method described by (Melgar and Bock, 2015), which allows for flexible rupture timing across the fault by assigning multiple overlapping source time functions to each subfault: eight 50% overlapping triangles with 4 s rise time allowed for each. This 4 s rise time is consistent with what is expected from a M7.8 earthquake from analysis of global earthquakes (Melgar and Hayes, 2017). Observed ground displacement time series from integrated strong motion and the pixel offsets from SAR are jointly inverted to estimate the spatial and temporal distribution of fault slip. To ensure balanced contributions from each data type, we normalized the residuals by the L2 norm of each dataset, effectively weighting them equally in the objective function (e.g. Melgar et al., 2020). Rupture initiation was assumed to occur at the hypocenter reported by the U.S. Geological Survey at 2025-03-28 06:20:52 (UTC) at 22.001°N, 95.925°E, and 10.0 km depth. Several maximum allowable rupture speeds were tested, ranging from 3.0 to 6.0 km/s, to explore sensitivity of the inversion to this constraint. The inversion is stabilized using Tikhonov regularization and the final model was selected based on the L-curve criterion.

2.4 Paleoseismology

We document displacement and frequency of surface ruptures from historic and paleoseismic earthquakes on the Sagaing Fault at a site (Figure 1B, 5A) near the 2025 M7.8 epicenter NW of Mandalay. Paleoseismic results reported here are preliminary and from work carried out in the context of a field-training school funded by the Earth Observatory of Singapore and including students from Myanmar, five other SE Asian countries, China, and USA from 2016 to 2018. We chose a portion of the Sagaing Fault where the active trace diverges from the range front (Figure S2) and trends more westerly (northern two-thirds of Figure 5B), causing compression and uplifting low hills that block stream flow and thus rapidly accumulate young sediment that includes abundant ^{14}C samples and Buddhist-era artifacts we use for age control (Figure S3). Using drone imagery (Figure S2) and ground-based LiDAR, we mapped geomorphic offsets and excavated 18 trenches to reveal deformation associated with past earthquakes. An example of a bare trench-log can be seen in Figure S4. Here we focus on a group of trenches in the southern half of the area (central portions of Figures 5B, S2) where the age and displacement associated with the five surface ruptures before 2025 can be estimated.

We attempted to reconstruct the coseismic displacements at this site and can now compare the 2025 offsets to past ruptures. To estimate the vertical component of slip associated with prehistoric surface-rupturing earthquakes, we applied a geomorphic approach (Figure 6) based on the formation of colluvial wedges at fault scarps. Following a surface-rupturing event, the exposed scarp undergoes gravitational collapse and subsequent erosion, depositing a wedge-shaped body of debris on the downthrown block. Experimental and field observations demonstrate that the maximum thickness

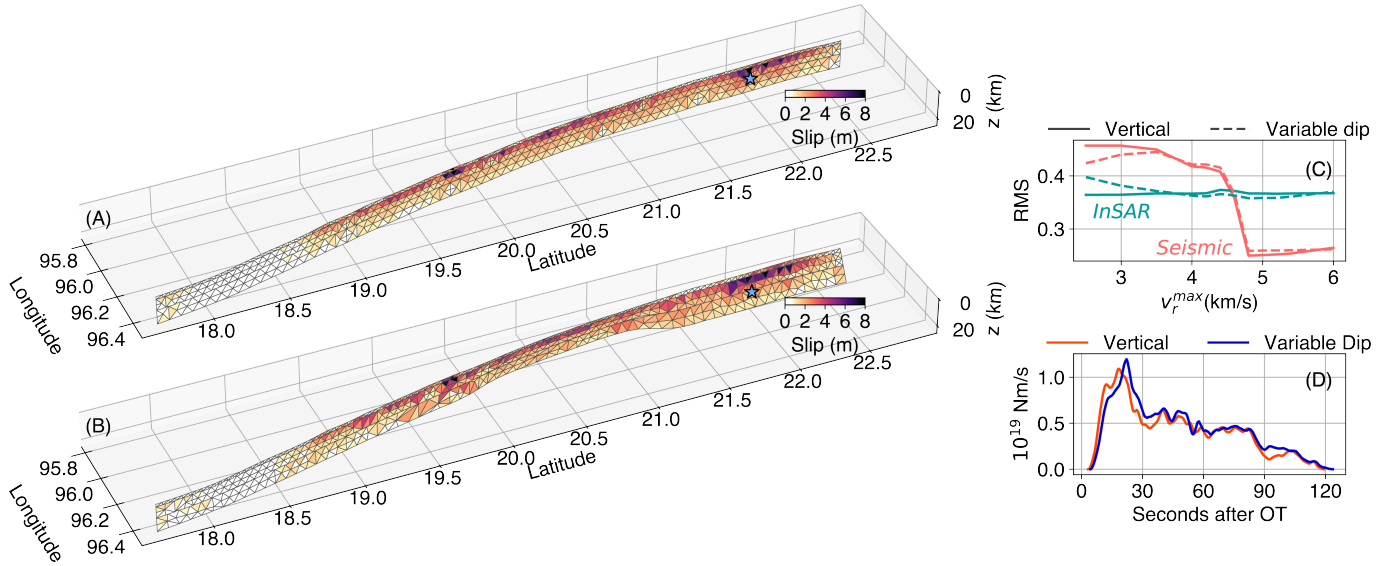

Figure 4 (A) Perspective view of the best-fit rupture model assuming a purely vertical geometry. Blue star is the assumed hypocenter. (B) same as (A) but with a variable-dip geometry. (C) RMS misfits averaged over all stations and image pixels as a function of maximum allowed rupture speed for both SAR pixel offsets and seismic data for each of the two geometries. Lowest misfits occur at 4.8 km/s. (D) Source time functions for the preferred models showing a rupture duration of 90-120 s.

of such a wedge is typically about half the height of the original fault scarp (Wallace, 1977; Nash, 1980; Avouac and Peltzer, 1993; Deng and Zhang, 2000).

We use this geometric relationship to infer the height of paleo-scarps—and by extension, the vertical displacement—by measuring the preserved maximum thickness of buried colluvial wedges in the trench exposures. This method has been applied in previous studies, notably by Klinger et al. (2003), who argued that colluvial wedges of ~0.8 m thickness corresponded to ~1.6 m of vertical slip during repeated events on a normal-faulting step-over along the North Anatolian Fault. Their analysis showed that wedge thicknesses can serve as reliable proxies for scarp height, particularly in settings where vertical displacement dominates and preservation conditions are favorable.

In our analysis, we adopt the same 2:1 ratio (scarp height to wedge thickness) as a first-order approximation of vertical offset for each scarp-forming event identified in the stratigraphy, which for for four of the five collectively measure 1.6 m in thickness (the youngest is too modified due to cultural activity associated with local agriculture). This yields an average of 40 cm per event (Figure 6A, B), so we infer that individual events have vertical displacement of ~80 cm. We note that this calculation neglects the youngest event which is heavily modified by agriculture. Given the orientation of this portion of the fault (measured across the eight walls in the map in Figure 6A, similar to the orientation at the trench site in Figure 5A) relative to the orientation of pure strike-slip portions nearby, we would expect the vertical to be about 20% of the horizontal, so the average horizontal displacement would be about 4 m. This is consistent with the 2025 rupture and fluvial sediments seen in the lowest wedge (blue in Figure 6C) that likely came from a small stream now followed by the road ~20 m to the north.

We are a working on a more complete 3D reconstruction of the wedges and fault traces using all eight exposures of the fault zone shown in the map in Figures 5B and 6A which will allow us to make a better determination of the thicknesses–and possibly offsets–of individual wedges and to put all of our ^{14}C samples into a single stratigraphic column to make the best age model possible.

3 Results and discussion

3.1 The Earthquake Source

The slip inversion results in Figure 4A, B show significant slip from the hypocenter north to ~22.2N and south to at least 18.5N for a full rupture length of ~450 km. Slip is highest between the surface and 10 km depth and tapers from there to 20 km. Depth averaged slip is ~3-5m across the rupture (e.g. Figure 5A) with localized small patches of higher amplitude slip as great as 7-8 m. The total magnitude for the event from inversion, depending on whether the vertical or variable dip geometry is preferred, is M 7.75 - 7.79. Thus the long rupture length is somewhat anomalous compared to the mean expected length of 186 km for this magnitude from the probabilistic scaling laws of Blaser et al. (2010), placing it at the 98th percentile of expected rupture lengths. Similarly, considering the scaling relationships for source area of strike-slip events from Thingbaijam et al. (2017) and the assumed seismogenic depth of 20 km, we would expect a rupture length of ~300 km for this magnitude. By all these metrics, the event is remarkably long.

In terms of its kinematics, even without an analysis of the inversion, we can conclude the rupture is most likely super-shear. Station NPW on the surface trace of the fault (Figures 1A, 2) shows a clear slip pulse with large fault-parallel ground motions. The dashed lines on Figure 2 indicate how quickly a rupture front would

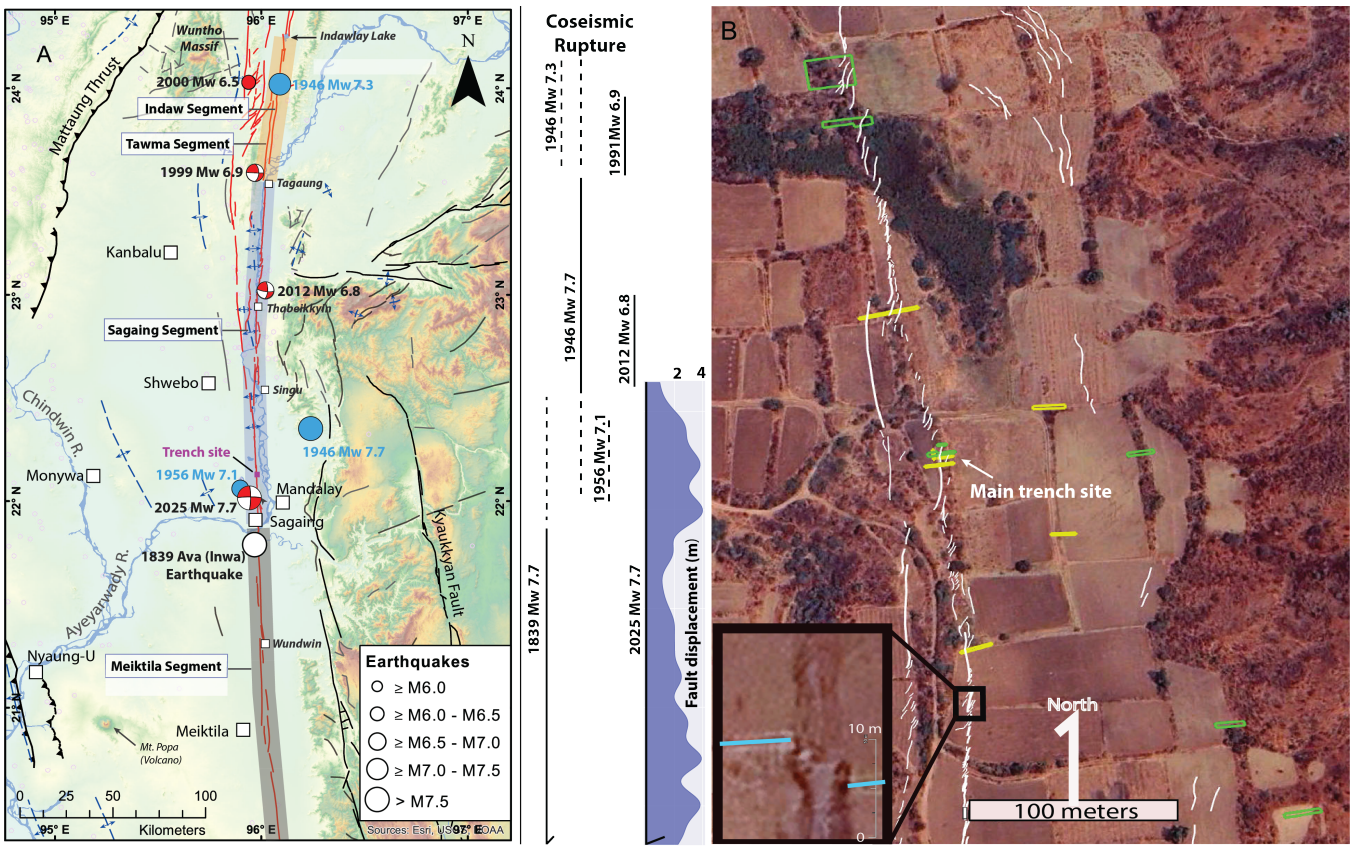

Figure 5 (A) Historic earthquakes and paleoseismic site plotted on a geologic map of the Sagaing Fault (updated from Wang et al., 2014). Regional location shown in Figure 1B. Colored rectangles along the fault are the Indaw, Tawma, Sagaing, and Meiktila fault segments (Wang et al., 2014). Blue circles are inferred event hypocenters and red beachballs the mechanisms, for historical earthquakes from Hurukawa and Maung (2011) and Wang et al. (2014) and rupture extents of historic surface ruptures (dashed where uncertain) are on right side with along-strike displacement shown for 2025. Shown as well is the depth-averaged displacement from our preferred slip model. For 2025 the beachball is at the location of the hypocenter. (B) Post-earthquake Google Earth image acquired April, 2025 of the paleoseismic study site centered at 22.0090°N, 95.9826°E. White lines are visible surface ruptures, green are 2016 trenches, yellow are 2018 trenches, and box in SW corner locates one of many 4-5m offsets (blue lines are an offset trail) in 2025 along this portion of the fault. Trenches east of the main trace were excavated to confirm that geomorphic lineaments were not recently active, although scattered cracks from the 2025 rupture indicate that the range front is not completely inactive. Westernmost white lines indicate cracks along the back edge of the uplifted hills that was only exposed in one trench. The images and analysis in Figure 6 are located at the location labeled "main trench site" and have the best evidence for the timing and displacement of recent earthquakes.

have to propagate from the catalog hypocenter along the Sagaing Fault to reach NPW. This simple analysis suggests strongly that the pulse needs to be traveling at just under 5 km/s. This is in fact confirmed by the slip inversion results shown in Figure 4C which shows that the best RMS misfit to the regional strong-motion data is for a maximum rupture speed of 4.8 km/s. Indeed, at this rupture speed, the fits to the strong-motion waveforms (Figure S5), in particular station NPW, are quite good with the exception of the north and vertical components at station YGN at the southern terminus of the rupture (Figure 1B). As noted by Thiam et al. (2017) YGN is on the sediment from the Ayeyarwady and Sitang River deltas and likely has significant site amplification effects we are not capturing with our simple 1D velocity structure. Likewise, both ascending and descending SAR pixel offset scenes show good fits (Figure 3) with no significant biases in the residual patterns. These results do not allow us to say conclusively whether the vertical or variable dip geometry are preferred as they both fit the data at similar levels. Finally, we note that given the significant fault length, and despite the fast rupture propagation, the source duration is long (Figure 4D) lasting as much as 120 s. However, the moment released between 90 and 120 s is from slip at the southern terminus of the rupture and most likely spurious and an attempt by the inversion process to fit later arrivals at YGN, the southernmost site. The more likely source duration is closer to ~90 s.

3.2 A history of overlapping ruptures at the northern terminus of the 2025 event

Preliminary results from our mapping, trenches, and age control provide evidence for five surface ruptures that occurred at the site in the ~1000 years before 2025. This includes post-bomb ^{14}C dates consistent with either or both of the 1946/1956 sequence, and stratigraphically consistent ^{14}C representing the 1839 event. Buddhist-era pottery limits the past five events to less

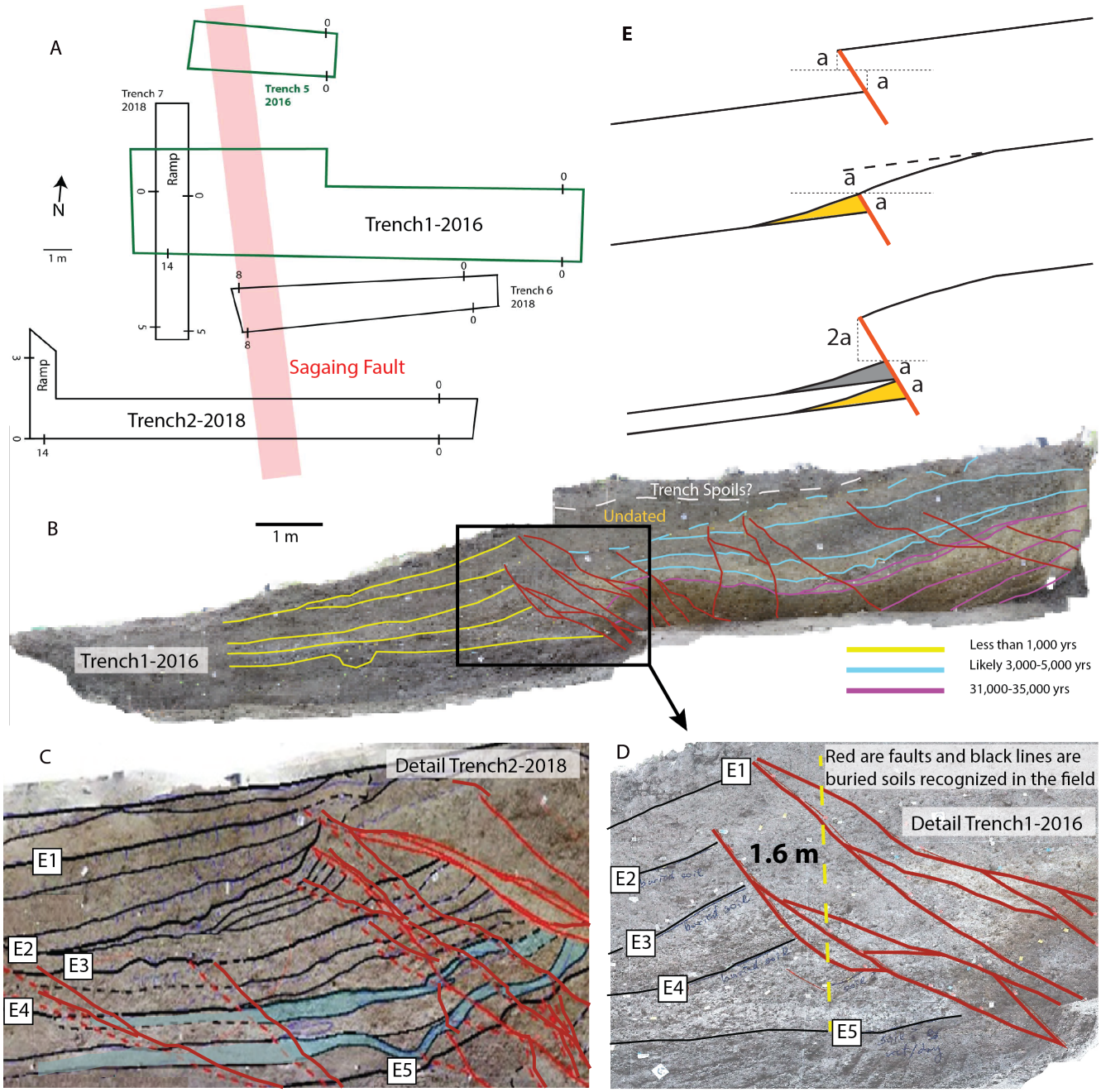

Figure 6 (A) Simplified map of trenches excavated between 2016-2018 (location is in Figure 5) (B) Example of a trench (Trench1-2016) across the main trace. (C) Detail of the main fault zone from Trench2-2018. We recognize 5 pre-2025 ruptures (E1-E5) and collected abundant charcoal and cow bones for ^{14}C samples and pottery to date the ruptures. Upward termination of individual fault surfaces and soil-capped colluvial wedges generated by individual earthquakes allow us to characterize and date events from the past 1000 years. Light blue layers between E4 & E5 are from a small stream laterally offset 20 m from the fault (Figure 5B), suggesting average lateral slip of 4-5 m per event. (D) Same as (C) for Trench1-2016, location of both in red shaded area in (A). The aggregate width of colluvial wedges for E2-E5 was measured 1.6 m corresponding 40 cm per wedge per event. (E) Cartoon (modified from Klinger et al., 2003) shows the typical relationship between the vertical component of slip and resulting scarp wedge thickness, suggesting 80 cm of vertical slip per event, similar to the 2025 scarp at the site.

than ~1000 years (Guy, 1990). Although displacement per event, based largely on colluvial wedge thickness and the ratio of vertical to horizontal slip (Figure 6E), appears to vary by at least a factor of 2, the average displacement of the previous five events (or sequence if close in time like 1946/56) is 4-5 meters, similar to the 2025 rupture displacement at the site (see Figure 5A, and post-event reconnaissance photos in Figure S7).

This last point is notable: at the location of our trenches (Figures 5, 6) several ruptures overlap. For an average slip rate of 20 mm/yr, the 4-5 m of coseismic slip on this segment of the fault inferred from paleoseismology and observed in 2025 requires 200-250 yrs to accumulate. That time is similar to the inter-event time we report here, as seen at the trenches. However, if the trench site is in an "overlap region" of Sagaing Fault rup-

tures, we might expect less periodic or regular behavior than suggested by this simple relationship. Whether large ruptures on major continental transforms cluster, are random, or are quasi-periodic has been the subject of debate (e.g. Scharer et al., 2010). Ongoing work on a 3D reconstruction and age model including all eight trench walls will help elucidate the detailed timing and displacement history here.

Furthermore, it is worth speculating on whether the short segment of the fault surrounding Mandalay is routinely the initiation point of large ruptures. Based on the paleoseismic record, with the new data from the 2025 rupture to supplement it, it appears that this portion of the fault often nucleates large ruptures that propagate either north or south and thus are centered more north (1946) or south (1839 & 2025) of the site (see epicenters in Figure 5).

Finally, we point out that the historic events and the 2025 earthquake suggest that the boundary between the Sagaing and Meiktila segments of the fault (Figure 5A) is rather diffuse. The inferred history shows that events that rupture both north and south overlap near the trench site. This suggests that the boundary is not a strict barrier beyond which only ruptures to the north or to the south exclusively occur. Rather, the ruptures that overlap at this trench can be north propagating, south propagating, and throughgoing (as in 2025). Whether other segments behave likewise is at present unknown and is further evidence of the need for more concerted paleoseismic work along the entirety of the fault.

3.3 Implications for hazards

The super-shear kinematics of this event add to the recent observations of similar behavior in other large transform faults such as the 2018 Palu, 2021 Maduo, and 2023 Türkiye earthquakes (Bao et al., 2019; Zhang et al., 2022; Melgar et al., 2023). How super-shear kinematics affect ground motion can be complex: modeling has shown that super-shear source processes can reduce ground motion immediately adjacent to the fault but increase it elsewhere (Dunham and Bhat, 2008; Andrews, 2010). These observations and models argue that super-shear ruptures are more common than previously considered and potentially not captured correctly in ground motion models. While it is difficult to interpret them without ambiguity, the "Did You Feel It Reports" from the USGS are biased high (U.S. Geological Survey, 2025), meaning they systematically indicate stronger than expected shaking for this event when compared to ground motion models. Is this due to the super-shear kinematics? And, can we expect all large events on this fault system to always exhibit this behavior? More work is needed to determine whether these source effects would impact seismic hazard estimates and, if so, to develop tools to appropriately represent them.

In terms of future hazards calculations for the Sagaing Fault, it is difficult to say what this event foretells for the region. Significant amounts of slip have been released and, significantly, most of the 2025 rupture last slipped in 1839. That inter-event interval allows for 3.8 m of slip deficit, most, if not all, of which would have been released in 2025. However, as evidenced by the event clusters in the trenches near Mandalay, it is plausible that slip deficit from earlier on in the seismic cycle remains available and unused. Without further paleoseismology elsewhere on the fault it is not feasible to say with any confidence whether the 2025 rupture significantly reduces hazard.

Conceptually, however, from simple Coulomb stress triggering arguments, and as seen on other transform systems, most famously in the Northern Anatolian fault (e.g., Stein et al., 1997), it would seem that the southern segments of the fault adjacent to the terminus of the 2025 rupture are of most concern: they have the fewest historic events and likely a large accumulated slip deficit. The last rupture here was an ~M7.2 earthquake in 1930 (Tsutsumi and Sato, 2009) and cumulative recurrence intervals for this segment have been inferred to be as short as 90-115 years (Wang et al., 2011). This interpretation is, of course, complicated by some partitioning of strain from the southern Sagaing Fault onto other sub-parallel faults (e.g. Tin et al., 2022). Whatever the case, the region is populous (Figure 1A) and this enormous exposure, when combined with precarious construction practices, continues to place the Sagaing Fault as potentially one of the most deadly continental transform faults in the world.

4 Conclusions

The 2025 Mw 7.8 earthquake along the central Sagaing Fault represents one of the most significant and destructive seismic events in Southeast Asia in recent history. Our joint kinematic inversion of regional strong motion and SAR pixel offset data reveals a ~450 km rupture with 3–5 m of average slip and supershear rupture propagation at ~4.8 km/s. This event adds to a growing list of well-documented supershear ruptures on major continental strike-slip faults. At a key paleoseismic site near the epicenter, we document evidence for five past surface-rupturing earthquakes over approximately the past millennium with comparable displacement, indicating repeated rupture of this portion of the fault and suggesting that this section of the Sagaing Fault is both a persistent nucleation zone and a locus of overlapping ruptures. These findings challenge models of strict fault segmentation and point to the need for reevaluation of seismic hazard across the broader fault system. The densely populated corridor along the Sagaing Fault remains acutely vulnerable, and our results underscore the urgent need for improved hazard mapping, infrastructure resilience, and expanded paleoseismic investigations across the fault's length.

Acknowledgements

We thank Kerry Sieh for his generous support and advocacy in funding fieldwork through the Earth Observatory of Singapore at Nanyang Technological University, and for discussions of paleoseismology of the Sagaing Fault. We woud also like to thank Paul Tapponnier for his insightful comments and suggestion before the fieldwork and to the Myanmar Earthquake Committee, and

the Myanmar Geosciences Society for their support in the fieldwork. This work was partially funded by NASA grant 23-ESI23-0012 to the University of Oregon and JPL teams. Part of the research was carried out at the Jet Propulsion Laboratory, California Institute of Technology, under a contract with the National Aeronautics and Space Administration (80NM0018D0004). We acknowledge support as well from National Science and Technology Council grants 112-2116-M-002-007 and 113-2116-M-002 –028 to YW.

Data and code availability

Supplementary Figures S1-S7, as well as all data needed to run the inversion and inversion results, are available in our Zenodo supplement (Melgar, 2025). Strong motion data for stations KTN, NGU and YGN is from Network MM operated by the Myanmar Department of Meteorology and Hydrology - National Earthquake Data Center (2016). Data for station NPW is from network GE from GEOFON Data Centre (1993). Kinematic slip inversion code MudPy is open source archived at Melgar et al. (2021) and available at https://github.com/UO-Geophysics/MudPy. This work utilized modified Copernicus data from Sentinel-1A/B and Sentinel-2A, -2B, and -2C satellites acquired and provided by the European Space Agency. Original Sentinel-1 and Sentinel-2 data are available from the Copernicus Data Space Ecosystem (https://dataspace.copernicus.eu/), and Sentinel-1 data are also available from the Alaska Satellite Facility data archive (https://asf.alaska.edu/asfsardaac/). Processed optical and SAR pixel offset data are available in our Zenodo supplement and through the aria-share repository at https://aria-share.jpl.nasa.gov/20250328_Myanmar_EQ/ .

Competing interests

The authors declare that they have no competing interests.

References

Andrews, D. Ground motion hazard from supershear rupture. *Tectonophysics*, 493(3 – 4):216 – 221, Oct. 2010. doi: 10.1016/j.tecto.2010.02.003.

Avouac, J. and Peltzer, G. Active tectonics in southern Xinjiang, China: Analysis of terrace riser and normal fault scarp degradation along the Hotan-Qira Fault System. *Journal of Geophysical Research: Solid Earth*, 98(B12):21773 – 21807, Dec. 1993. doi: 10.1029/93jb02172.

Avouac, J.-P. and Leprince, S. *Geodetic Imaging Using Optical Systems*, page 387 – 424. Elsevier, 2015. doi: 10.1016/b978-0-444-53802-4.00067-1.

Bao, H., Ampuero, J.-P., Meng, L., Fielding, E. J., Liang, C., Milliner, C. W. D., Feng, T., and Huang, H. Early and persistent supershear rupture of the 2018 magnitude 7.5 Palu earthquake. *Nature Geoscience*, 12(3):200 – 205, Feb. 2019. doi: 10.1038/s41561-018-0297-z.

Bato, M. G., Lundgren, P., Pinel, V., Solidum Jr., R., Daag, A., and Caahulogan, M. The 2020 eruption and large lateral dike emplacement at Taal volcano, Philippines: Insights from satellite radar data. *Geophysical Research Letters*, 48(7), 2021. doi: 10.1029/2021GL092803.

Blaser, L., Kruger, F., Ohrnberger, M., and Scherbaum, F. Scaling Relations of Earthquake Source Parameter Estimates with Special Focus on Subduction Environment. *Bulletin of the Seismological Society of America*, 100(6):2914 – 2926, Dec. 2010. doi: 10.1785/0120100111.

Bondár, I., Myers, S. C., Engdahl, E. R., and Bergman, E. A. Epicentre accuracy based on seismic network criteria. *Geophysical Journal International*, 156(3):483 – 496, Mar. 2004. doi: 10.1111/j.1365-246x.2004.02070.x.

Casu, F., Manconi, A., Pepe, A., and Lanari, R. Deformation Time-Series Generation in Areas Characterized by Large Displacement Dynamics: The SAR Amplitude Pixel-Offset SBAS Technique. *IEEE Transactions on Geoscience and Remote Sensing*, 49(7):2752 – 2763, July 2011. doi: 10.1109/tgrs.2010.2104325.

Curray, J. R. Tectonics and history of the Andaman Sea region. *Journal of Asian Earth Sciences*, 25(1):187 – 232, Apr. 2005. doi: 10.1016/j.jseaes.2004.09.001.

Deng, Q. and Zhang, P. Colluvial wedges associated with pre-historical reverse faulting paleoearthquakes. *Chinese Science Bulletin*, 45(17):1598 – 1604, Sept. 2000. doi: 10.1007/bf02886221.

Drusch, M., Del Bello, U., Carlier, S., Colin, O., Fernandez, V., Gascon, F., Hoersch, B., Isola, C., Laberinti, P., Martimort, P., Meygret, A., Spoto, F., Sy, O., Marchese, F., and Bargellini, P. Sentinel-2: ESA' s Optical High-Resolution Mission for GMES Operational Services. *Remote Sensing of Environment*, 120:25 – 36, May 2012. doi: 10.1016/j.rse.2011.11.026.

Dunham, E. M. and Bhat, H. S. Attenuation of radiated ground motion and stresses from three-dimensional supershear ruptures. *Journal of Geophysical Research: Solid Earth*, 113(B8), Aug. 2008. doi: 10.1029/2007jb005182.

Dziewonski, A. M. and Anderson, D. L. Preliminary reference Earth model. *Physics of the Earth and Planetary Interiors*, 25(4):297 – 356, June 1981. doi: 10.1016/0031-9201(81)90046-7.

Earle, P. S., Wald, D. J., Jaiswal, K. S., Allen, T. I., Hearne, M. G., Marano, K. D., Hotovec, A. J., and Fee, J. Prompt Assessment of Global Earthquakes for Response (PAGER): A System for Rapidly Determining the Impact of Earthquakes Worldwide. Open-file report, US Geological Survey, 2009. doi: 10.3133/ofr20091131.

Ekström, G., Nettles, M., and Dziewoński, A. The global CMT project 2004 – 2010: Centroid-moment tensors for 13,017 earthquakes. *Physics of the Earth and Planetary Interiors*, 200 – 201:1 – 9, June 2012. doi: 10.1016/j.pepi.2012.04.002.

Gahalaut, V. K. and Gahalaut, K. Burma plate motion. *Journal of Geophysical Research: Solid Earth*, 112(B10), Oct. 2007. doi: 10.1029/2007jb004928.

Gardner, A. S., Moholdt, G., Scambos, T., Fahnstock, M., Ligtenberg, S., van den Broeke, M., and Nilsson, J. Increased West Antarctic and unchanged East Antarctic ice discharge over the last 7 years. *The Cryosphere*, 12(2):521 – 547, Feb. 2018. doi: 10.5194/tc-12-521-2018.

GEOFON Data Centre. GEOFON Seismic Network [Data set], 1993.

Guy, J. *Ceramic Traditions of SE Asia*. Oxford University Press, 1990.

Hurukawa, N. and Maung, P. M. Two seismic gaps on the Sagaing Fault, Myanmar, derived from relocation of historical earthquakes since 1918. *Geophysical Research Letters*, 38(1), Jan. 2011. doi: 10.1029/2010gl046099.

Inoue, N., Yamaguchi, R., Yagi, Y., Okuwaki, R., Enescu, B., and Tadapansawut, T. A multiple asymmetric bilateral rupture sequence derived from the peculiar tele-seismic P-waves of the 2025 Mandalay, Myanmar earthquake. 4(1), 2025. doi:

10.26443/seismica.v4i1.1691.

Kearse, J. and Kaneko, Y. Curved Fault Slip Captured by CCTV Video During the 2025 M w 7.7 Myanmar Earthquake. *The Seismic Record*, 5(3), 2025. doi: 10.1785/0320250024.

Kennett, B. L. N. and Engdahl, E. R. Traveltimes for global earthquake location and phase identification. *Geophysical Journal International*, 105(2):429 – 465, May 1991. doi: 10.1111/j.1365-246x.1991.tb06724.x.

Klinger, Y., Sieh, K., Altunel, E., Akoglu, A., Barka, A., Dawson, T., Gonzalez, T., Meltzner, A., and Rockwell, T. Paleoseismic Evidence of Characteristic Slip on the Western Segment of the North Anatolian Fault, Turkey. *Bulletin of the Seismological Society of America*, 93(6):2317 – 2332, Dec. 2003. doi: 10.1785/0120010270.

Lai, S.-T., Oo, K. M., Htwe, Y. M. M., Yi, T., Than, H. H., Than, O., Min, Z., Oo, T. M., Maung, P. M., Bindi, D., Cotton, F., Evans, P. L., Heinloo, A., Hillmann, L., Saul, J., Sens-Schoenfelder, C., Strollo, A., Tilmann, F., Weatherill, G., Yen, M.-H., Zaccarelli, R., Zieke, T., and Milkereit, C. Capacity Building Enables Unique Near-Fault Observations of the destructive 2025 Mw 7.7 Myanmar Earthquake. Unpublished, preprint, Apr. 2025. doi: 10.5194/essd-2025-216.

Le Dain, A. Y., Tapponnier, P., and Molnar, P. Active faulting and tectonics of Burma and surrounding regions. *Journal of Geophysical Research: Solid Earth*, 89(B1):453 – 472, Jan. 1984. doi: 10.1029/jb089ib01p00453.

Lebakula, V., Epting, J., Moehl, J., Stipek, C., Adams, D., Reith, A., Kaufman, J., Gonzales, J., Reynolds, B., Basford, S., Martin, A., Buck, W., Faxon, A., Cunningham, A., Roy, A., Barbose, Z., Massaro, J., Walters, S., Woody, C., Iman, A., Wilkins, A., Powell, E., and Urban, M. LandScan Silver Edition, 2024. doi: 10.48690/1531770.

Lei, Y., Gardner, A., and Agram, P. Autonomous Repeat Image Feature Tracking (autoRIFT) and Its Application for Tracking Ice Displacement. *Remote Sensing*, 13(4):749, Feb. 2021. doi: 10.3390/rs13040749.

Lindsey, E. O., Wang, Y., Aung, L. T., Chong, J.-H., Qiu, Q., Mallick, R., Feng, L., Aung, P. S., Tin, T. Z. H., Min, S. M., Bradley, K., Than, O., Oo, K. M., Thant, M., Masson, F., Bürgmann, R., and Hill, E. M. Active subduction and strain partitioning in western Myanmar revealed by a dense survey GNSS network. *Earth and Planetary Science Letters*, 622:118384, Nov. 2023. doi: 10.1016/j.epsl.2023.118384.

Mallick, R., Lindsey, E. O., Feng, L., Hubbard, J., Banerjee, P., and Hill, E. M. Active Convergence of the India-Burma-Sunda Plates Revealed by a New Continuous GPS Network. *Journal of Geophysical Research: Solid Earth*, 124(3):3155 – 3171, Mar. 2019. doi: 10.1029/2018jb016480.

Maung, H. Transcurrent movements in the Burma – Andaman Sea region. *Geology*, 15(10):911 – 912, 1987.

Maurin, T., Masson, F., Rangin, C., Min, U. T., and Collard, P. First global positioning system results in northern Myanmar: Constant and localized slip rate along the Sagaing fault. *Geology*, 38(7):591 – 594, June 2010. doi: 10.1130/g30872.1.

Melgar, D. Supplementary material for "Supershear source model of the 2025 M7.8 Myanmar earthquake and paleoseismology of the Sagaing Fault: regions of significant overlap with past earthquakes [Data set], 2025. doi: 10.5281/zenodo.15529795.

Melgar, D. and Bock, Y. Kinematic earthquake source inversion and tsunami runup prediction with regional geophysical data. *Journal of Geophysical Research: Solid Earth*, 120(5):3324 – 3349, May 2015. doi: 10.1002/2014jb011832.

Melgar, D. and Hayes, G. P. Systematic Observations of the Slip Pulse Properties of Large Earthquake Ruptures. *Geophysical Research Letters*, 44(19):9691 – 9698, Oct. 2017. doi: 10.1002/2017gl074916.

Melgar, D., Ganas, A., Taymaz, T., Valkaniotis, S., Crowell, B. W., Kapetanidis, V., Tsironi, V., Yolsal-Çevikbilen, S., and Öcalan, T. Rupture kinematics of 2020 January 24 Mw 6.7 Doğanyol-Sivrice, Turkey earthquake on the East Anatolian Fault Zone imaged by space geodesy. *Geophysical Journal International*, 223 (2):862 – 874, July 2020. doi: 10.1093/gji/ggaa345.

Melgar, D., Lin, T., Qingkai Kong, Christineruhl, and Marfito, B. dmelgarm/MudPy: v1.3, 2021. doi: 10.5281/ZENODO.5397091.

Melgar, D., Taymaz, T., Ganas, A., Crowell, B., Öcalan, T., Kahraman, M., Tsironi, V., Yolsal-Çevikbil, S., Valkaniotis, S., Irmak, T. S., Eken, T., Erman, C., Özkan, B., Dogan, A. H., and Altuntaş, C. Sub- and super-shear ruptures during the 2023 Mw 7.8 and Mw 7.6 earthquake doublet in SE Türkiye. *Seismica*, 2(3), Mar. 2023. doi: 10.26443/seismica.v2i3.387.

Mon, C. T., Gong, X., Wen, Y., Jiang, M., Chen, Q., Zhang, M., Hou, G., Thant, M., Sein, K., and He, Y. Insight Into Major Active Faults in Central Myanmar and the Related Geodynamic Sources. *Geophysical Research Letters*, 47(8), Apr. 2020. doi: 10.1029/2019gl086236.

Morley, C. and Arboit, F. Dating the onset of motion on the Sagaing fault: Evidence from detrital zircon and titanite U-Pb geochronology from the North Minwun Basin, Myanmar. *Geology*, 47(6):581 – 585, Apr. 2019. doi: 10.1130/g46321.1.

Myanmar Department of Meteorology and Hydrology - National Earthquake Data Center. Myanmar National Seismic Network, 2016. doi: 10.7914/SN/MM.

Nash, D. B. Morphologic Dating of Degraded Normal Fault Scarps. *The Journal of Geology*, 88(3):353 – 360, May 1980. doi: 10.1086/628513.

National Research Council. *Tools and methods for estimating populations at risk from natural disasters and complex humanitarian crises*. National Academies Press, 1st edition, 2007.

Panda, D., Kundu, B., Gahalaut, V. K., and Rangin, C. Crustal deformation, spatial distribution of earthquakes and along strike segmentation of the Sagaing Fault, Myanmar. *Journal of Asian Earth Sciences*, 166:89 – 94, Oct. 2018. doi: 10.1016/j.jseaes.2018.07.029.

Pasyanos, M. E., Masters, T. G., Laske, G., and Ma, Z. LITHO1.0: An updated crust and lithospheric model of the Earth. *Journal of Geophysical Research: Solid Earth*, 119(3):2153 – 2173, Mar. 2014. doi: 10.1002/2013jb010626.

Pathier, E., Fielding, E. J., Wright, T. J., Walker, R., Parsons, B. E., and Hensley, S. Displacement field and slip distribution of the 2005 Kashmir earthquake from SAR imagery. *Geophysical Research Letters*, 33(20), Oct. 2006. doi: 10.1029/2006gl027193.

Pornsopin, P., Pananont, P., Furlong, K. P., and Sandvol, E. Sensor orientation of the TMD seismic network (Thailand) from P-wave particle motions. *Geoscience Letters*, 10(1), May 2023. doi: 10.1186/s40562-023-00278-7.

Rosen, P., Gurrola, E., Sacco, G., and Zebker, H. The InSAR scientific computing environment. In *EUSAR 2012; 9th European conference on synthetic aperture radar*, page 730 – 733. VDE, 2012.

Scharer, K. M., Biasi, G. P., Weldon, R. J., and Fumal, T. E. Quasi-periodic recurrence of large earthquakes on the southern San Andreas fault. *Geology*, 38(6):555 – 558, June 2010. doi: 10.1130/g30746.1.

Shi, X., Wang, Y., Sieh, K., Weldon, R., Feng, L., Chan, C., and Liu-Zeng, J. Fault Slip and GPS Velocities Across the Shan Plateau Define a Curved Southwestward Crustal Motion Around the Eastern Himalayan Syntaxis. *Journal of Geophysical Research: Solid Earth*, 123(3):2502 – 2518, Mar. 2018. doi:

10.1002/2017jb015206.

Socquet, A., Vigny, C., Chamot-Rooke, N., Simons, W., Rangin, C., and Ambrosius, B. India and Sunda plates motion and deformation along their boundary in Myanmar determined by GPS. *Journal of Geophysical Research: Solid Earth*, 111(B5), May 2006. doi: 10.1029/2005jb003877.

Steckler, M. S., Mondal, D. R., Akhter, S. H., Seeber, L., Feng, L., Gale, J., Hill, E. M., and Howe, M. Locked and loading megathrust linked to active subduction beneath the Indo-Burman Ranges. *Nature Geoscience*, 9(8):615 – 618, July 2016. doi: 10.1038/ngeo2760.

Stein, R. S., Barka, A. A., and Dieterich, J. H. Progressive failure on the North Anatolian fault since 1939 by earthquake stress triggering. *Geophysical Journal International*, 128(3), 1997. doi: 10.1111/j.1365-246x.1997.tb05321.x.

Strozzi, T., Luckman, A., Murray, T., Wegmuller, U., and Werner, C. Glacier motion estimation using SAR offset-tracking procedures. *IEEE Transactions on Geoscience and Remote Sensing*, 40 (11):2384 – 2391, Nov. 2002. doi: 10.1109/tgrs.2002.805079.

Thein, M., Mying, T., Tun, S. T., and Swe, T. L. Earthquake and Tsunami Hazard in Myanmar. *Journal of Earthquake and Tsunami*, 03(02):43 – 57, June 2009. doi: 10.1142/s1793431109000482.

Thiam, H. N., Htwe, Y. M. M., Kyaw, T. L., Tun, P. P., Min, Z., Htwe, S. H., Aung, T. M., Lin, K. K., Aung, M. M., Cristofaro, J. d., Franke, M., Radman, S., Lepiten, E., Wolin, E., and Hough, S. E. A Report on Upgraded Seismic Monitoring Stations in Myanmar: Station Performance and Site Response. *Seismological Research Letters*, 88(3):926 – 934, Mar. 2017. doi: 10.1785/0220160168.

Thingbaijam, K. K. S., Martin Mai, P., and Goda, K. New Empirical Earthquake Source-Scaling Laws. *Bulletin of the Seismological Society of America*, 107(5):2225 – 2246, Sept. 2017. doi: 10.1785/0120170017.

Tin, T. Z. H., Nishimura, T., Hashimoto, M., Lindsey, E. O., Aung, L. T., Min, S. M., and Thant, M. Present-day crustal deformation and slip rate along the southern Sagaing fault in Myanmar by GNSS observation. *Journal of Asian Earth Sciences*, 228:105125, May 2022. doi: 10.1016/j.jseaes.2022.105125.

Tsutsumi, H. and Sato, T. Tectonic Geomorphology of the Southernmost Sagaing Fault and Surface Rupture Associated with the May 1930 Pegu (Bago) Earthquake, Myanmar. *Bulletin of the Seismological Society of America*, 99(4):2155 – 2168, July 2009. doi: 10.1785/0120080113.

Tun, S. T. and Watkinson, I. M. The Sagaing Fault, Myanmar. *Geological Society, London, Memoirs*, 48(1):413 – 441, Jan. 2017. doi: 10.1144/m48.19.

U.S. Geological Survey. M 7.7 - 2025 Mandalay, Burma (Myanmar) Earthquake„ 2025. https://earthquake.usgs.gov/earthquakes/eventpage/us7000pn9s/pager.

U.S. Geological Survey Hazards Program. Advanced National Seismic System (ANSS) Comprehensive Catalog, 2017. doi: 10.5066/F7MS3QZH.

Vigny, C., Socquet, A., Rangin, C., Chamot-Rooke, N., Pubellier, M., Bouin, M., Bertrand, G., and Becker, M. Present-day crustal deformation around Sagaing fault, Myanmar. *Journal of Geophysical Research: Solid Earth*, 108, 2003. doi: 10.1029/2002jb001999.

Wald, D., Jaiswal, K., Marano, K., Earle, P., and Allen, T. *Advancements in Casualty Modelling Facilitated by the USGS Prompt Assessment of Global Earthquakes for Response (PAGER) System*, page 221 – 230. Springer Netherlands, Dec. 2010. doi: 10.1007/978-90-481-9455-1_15.

Wallace, R. Profiles and ages of young fault scarps, north-central Nevada, Geol. *Soc. Am. Bull*, 88:1267 – 1281, 1977.

Wang, Y., Sieh, K., Aung, T., Min, S., Khaing, S. N., and Tun, S. T. Earthquakes and slip rate of the southern Sagaing fault: insights from an offset ancient fort wall, lower Burma (Myanmar). *Geophysical Journal International*, 185(1):49 – 64, Feb. 2011. doi: 10.1111/j.1365-246x.2010.04918.x.

Wang, Y., Sieh, K., Tun, S. T., Lai, K., and Myint, T. Active tectonics and earthquake potential of the Myanmar region. *Journal of Geophysical Research: Solid Earth*, 119(4):3767 – 3822, Apr. 2014. doi: 10.1002/2013jb010762.

Xiong, X., Shan, B., Zhou, Y. M., Wei, S. J., Li, Y. D., Wang, R. J., and Zheng, Y. Coulomb stress transfer and accumulation on the Sagaing Fault, Myanmar, over the past 110 years and its implications for seismic hazard. *Geophysical Research Letters*, 44(10): 4781 – 4789, May 2017. doi: 10.1002/2017gl072770.

Xu, X., Tong, X., Sandwell, D. T., Milliner, C. W., Dolan, J. F., Hollingsworth, J., Leprince, S., and Ayoub, F. Refining the shallow slip deficit. *Geophysical Journal International*, 204(3):1843 – 1862, Feb. 2016. doi: 10.1093/gji/ggv563.

Yang, S., Xiao, Z., Wei, S., He, Y., Mon, C. T., Hou, G., Thant, M., Sein, K., and Jiang, M. New Insights Into Active Faults Revealed by a Deep-Learning-Based Earthquake Catalog in Central Myanmar. *Geophysical Research Letters*, 51(2), Jan. 2024. doi: 10.1029/2023gl105159.

Ye, L., Lay, T., and Kanamori, H. The 28 March 2025 M w 7.8 Myanmar Earthquake: Preliminary Analysis of an 𝔽 480 km Long Intermittent Supershear Rupture. *The Seismic Record*, 5(3), 2025. doi: 10.1785/0320250021.

Zhang, X., Feng, W., Du, H., Samsonov, S., and Yi, L. Supershear Rupture During the 2021 MW 7.4 Maduo, China, Earthquake. *Geophysical Research Letters*, 49(6), Mar. 2022. doi: 10.1029/2022gl097984.

Zhu, L. and Rivera, L. A. A note on the dynamic and static displacements from a point source in multilayered media. *Geophysical Journal International*, 148(3):619 – 627, Mar. 2002. doi: 10.1046/j.1365-246x.2002.01610.x.